



Seismic Performance of RC Circular Columns Strengthened with Self-compacting Concrete-Filled Steel Tubes

Zhaoqiang Zhang¹ · Yuxin Yi¹ · Tian Liao¹ · Xiaowei Li¹

Received: 14 January 2023 / Accepted: 9 June 2023 / Published online: 20 June 2023
© Korean Society of Steel Construction 2023

Abstract

To investigate the seismic performance of RC circular column strengthened with self-compacting concrete (SCC) -filled steel tubes (SCFST), nine specimens of height 1200 mm, varying with a cross-section shape of steel tube (external diameter: 218 mm, cross-section dimensions: 200 mm × 200 mm) were tested under axial load and cyclic lateral load. Three parameters, including the axial compression ratio, the cross-section shape of steel tube, and the embedding rebars ratio, were considered in the tests. The failure mode, hysteresis curves, skeleton curves, ductility, stiffness degradation, and energy-dissipation capacity were analysed. Experimental results showed that the bearing capacity and stiffness of the strengthened column were 5.4 and 9.08 times than that of the unstrengthened column respectively, and the improvement ratio of ductility and energy dissipation reached 123% and 85.7% respectively. The bearing capacity and stiffness of the square SCFST strengthened column was enhanced by 28.57% and 42.11% respectively, compared with the circular SCFST strengthened column. With the designed axial compression ratio increasing, the bearing capacity, initial stiffness, and energy dissipation capacity of strengthened columns increased by 17–39%, 21–60%, and 15–40% respectively, but the ductility coefficient decreased by 8.56–32.4%. The bearing capacity and energy dissipation of the specimen with an embedding rebars ratio of 0.06% increased by 7.5% and 9.31% respectively, but the ductility decreased by 12.81%. When the embedding rebars ratio was 0.1%, the reinforcement effect can be basically negligible.

Keywords Self-compacting concrete · Strengthened columns · Seismic performance

1 Introduction

Numerous buildings could not satisfy the reliability requirements for some reasons, including exceeding service life, functional degradation, poor construction quantity, and unpredictable disasters. To prolong the service life of the buildings and promote the sustainable development of society, it is essential to strengthen and retrofit structural members.

Commonly used strengthening methods, including pasting fiber composites, section enlargement, and outsourcing steel, have their advantages and disadvantages (Sezen & Miller, 2011; Shannag et al., 2002). To enhance the strengthening

effect, new materials and structures were adopted to ameliorate existing strengthening methods. Concrete-filled steel tube (CFST) is widely used in structural engineering due to the advantage of high strength and ductility, easy construction, and saving construction period (Mou et al., 2021; Tam et al., 2014). The steel tube can restraint core concrete, make it in a state of triaxial compressive stress, resulting in the improvement of concrete strength. Filling concrete can effectively prevent local buckling of steel tube. The interaction of steel tube and concrete reinforces structural members to resist bending moments, lateral forces, and shear forces (Abdalla et al., 2013; Abed et al., 2013; Valipour & Foster, 2010; Yu et al., 2016). Numerous scholars have conducted research on the mechanical properties of CFST columns. Gan et al. (2015) presented the composite response of circular CFST columns and found out that the restraint effect of the wrapped steel tube on the concrete obviously improved the bearing capacity and ductility of the short column, and the bearing capacity was improved with the axial compression ratio increasing. Zhou et al. (2008) tested 4 circular

✉ Zhaoqiang Zhang

✉ Yuxin Yi
y1187601058@163.com

¹ School of Civil Engineering and Architecture, Southwest University of Science and Technology, Mianyang 621010, China

CFST columns and 4 square CFST columns under cyclic load. It demonstrated that with the axial compression ratio and concrete strength increasing, the bearing capacity of CFST columns were improved, and the flexural capacity and ductility of circular CFST columns were apparently better than those of square CFST columns under the same axial compression ratio due to higher hoop effect provided by the circular steel tube. Wang et al. (2019) studied the seismic performance of circular CFST columns and found out that the ductility and energy dissipation of the CFST columns were enhanced with the designed axial compression ratio increasing. Foraboschi (2013, 2020) finished the analytical and exact modelling of composite flexural members, and further investigated the behaviour of steel members subjected to axial load and bending moment. It presented a formulation for predicting the ultimate combinations of axial force and bending moment, and indicated that the effects of loads acting on the deformed structure was caused by the interaction between axial and flexural force.

Based on extensive research on CFST columns, RC columns strengthened with CFST have the potential to be used in reinforcement field. Scholars have studied the mechanical performance of CFST strengthened columns and verified its reinforcement effect. Priestley et al. (1994a, b) presented a shear test of CFST strengthened columns and proposed that its bearing capacity, stiffness and ductility would be enhanced by strengthening with elliptical steel tube. Wang et al. (2021) indicated that the original RC column strengthened with CFST and cementitious grout jackets exhibited higher strength, stiffness and ductility than that of original RC column. Han et al. (2006) used CFST to strengthen the fire-damaged CFST columns and showed that the strength and stiffness of the fire-damaged CFST columns could be restored over the undamaged level of the specimens, and the ultimate load increased with the designed axial load ratio increasing. He et al. (2017, 2018) explored the compressive performance and seismic behaviour of RC column retrofitted with steel tube and recycled aggregate concrete (RAC). The results showed that the compressive capacity of strengthened columns was increased compared with unstrengthened columns. With the axial compressive ratio increasing, the bearing capacity, initial stiffness and ductility of the strengthened column were increased, but the improvement effect was weakened when the axial compressive ratio increased too great.

However, the concrete between the original RC column and steel tube can hardly vibrate and compact, resulting in voids and defects, which weaken the reinforcement effect (Lu et al., 2018). To overcome this problem, SCC is applied in CFST members because of its ultra-high fluidity, and it could flow through complex areas and evenly fill the formwork without mechanical vibration (Karimipour et al., 2020). Liao et al., (2021). Han et al. (2005) presented

the mechanical properties of SCC compacted with and without mechanical vibration. It indicated that the effect of the vibration or non-vibration of SCC was not obvious on the mechanical performance of SCFST strengthened columns, and SCFST strengthened columns showed better ultimate bearing capacity compared with the ordinary CFST strengthened columns. Studies have illustrated that SCFST is effective in enhancing the seismic behaviour of RC columns. Li et al. (2019) investigated the axial behaviour of SCFST strengthened columns and proposed that the bearing capacity, stiffness and ductility of the specimens were significantly enhanced by strengthening owing to the section enlargement and restriction provided by steel tube. Lu et al. (2015a, b, 2018) performed extensive research on the mechanical performance of SCFST strengthened columns, reported the effect of steel tube and SCC on enhancing the bearing capacity and ductility, and revealed that the bearing capacity of SCFST strengthened columns increased with the designed axial compression ratio increasing. Yan et al. (2019) tested 14 SCFST strengthened columns and 1 unstrengthened RC column under cyclic loading and found out that excessive axial compression ratio would weaken the reinforcement effect.

Besides, multiple studies showed that the interface treatment of new and old concrete plays an important role in the reinforcement effect (Guan et al., 2021; Jiang et al., 2014). Murugan & Sengupta, (2020) investigated the seismic performance of CFST strengthened columns, considering different interfaces treatment, including surface roughening, embedding dowel bars or bent shear connector bars. It showed that the shear forces and ultimate forces were found to improve effectively after strengthening the original column, and the specimens with embedding bent bars exhibited higher stiffness. Xue et al. (2014) indicated embedding rebar can enhance the shear resistance between the original RC column and SCC, but high embedding rebar ratio would damage the original RC column and reduce the effect of reinforcement.

Nevertheless, research programs were rarely conducted on the aspect about seismic performance of SCFST strengthened columns. To investigate seismic behaviour of SCFST strengthened columns, the cyclic test of nine specimens were presented. The effect of some parameters such as axial compression ratio, embedding rebars ratio, and the cross-section shape of steel tube were considered. The failure modes, hysteresis curves, skeleton curves, ductility, stiffness degradation, and energy-dissipation capacity of nine specimens were studied. It revealed that the strengthening method used in this paper exhibited excellent reinforcement effect under earthquake action, and provided reference significance for engineering practice.

2 Experimental Scheme

2.1 Design of Specimens

Nine specimens of height 1200 mm were fabricated, including an original RC column, three RC columns strengthened with SCC-filled circular steel tubes (SCFCST), and five RC columns strengthened with SCC-filled square steel tubes (SCFSST). The external diameter of circular steel tubes was 218 mm, and the cross-section dimensions of square steel tubes was 200 mm × 200 mm. All steel tubes had the same thickness of 3.5 mm. Each column was constructed together with an 800 mm × 700 mm × 500 mm RC footing to model the constraint. All of the original RC columns had the same diameter of 110 mm, and six longitudinal rebars with the diameter of 8 mm were evenly distributed in the circumference, and the diameter of hoop rebar was 6 mm. Furthermore, the spacing of the hoop rebar between dense areas and non-dense areas were 100 mm and 150 mm, respectively. Detailed information of the specimens is given in Fig. 1. The schematic of the behaviour of the reference structure

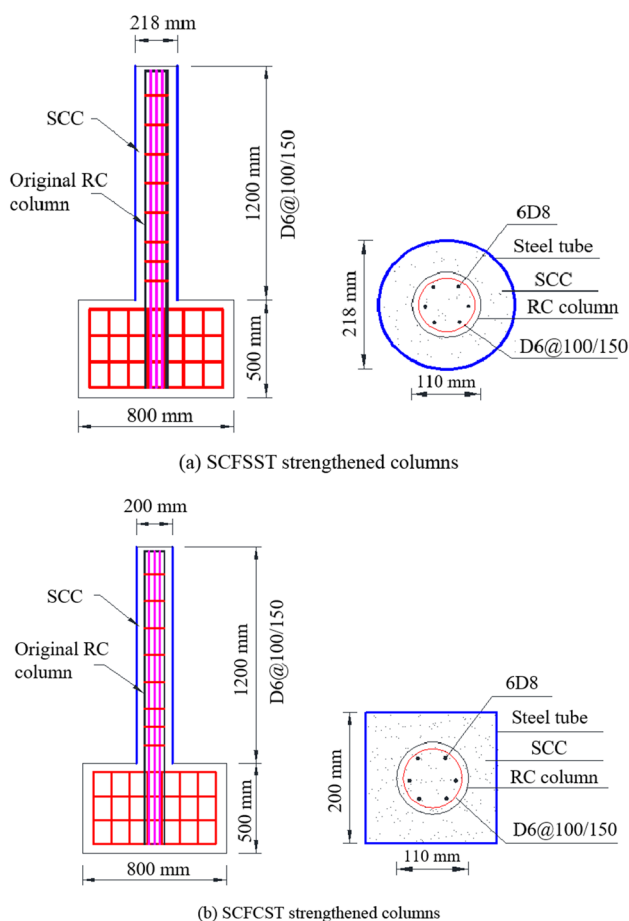


Fig. 1 Configurations and details of the specimens

subjected to axial load and bending moment is shown in Fig. 2. Table 1 lists the details of each column. Where, T , D and L are the steel tube thickness, the external diameter or side length of steel tube, and the valid height of column, respectively; n and N represent the axial compression ratio and the embedding rebars ratio, respectively.

For the specimens considering the embedding rebars rate, the interface treatment of embedding rebars at column bottom in addition to surface roughening was adopted to test specimens. The HPB300 rebars with diameter of 6 mm were embedded after roughening the RC column surface, with a total length of 40 mm. The specific process is as follows. Firstly, the positions of embedding rebars were marked on the original RC column surface. Secondly, the holes with the drilling depth of 20 mm were punched at the column bottom, and the drilling direction was perpendicular to the column surface. Then, the epoxy resin adhesive was injected in the holes. Finally, the rebars were embedded into the holes. The embedding rebars ratio is the rate of the sum of the cross-sectional area of the embedded rebars to the side surface areas of the original RC column. For the specimen with 0.10% embedding rebars ratio, there were three columns and five rows of embedded rebars with the interval of 200 mm and 36.7 mm in each row and column respectively, and the rebars were embedded from 200 mm at column bottom, and a total of 15 rebars were embedded. For the specimen with 0.06% embedding rebars ratio, there were three columns and three rows of embedded rebars with the interval of 400 mm and 36.7 mm in each row and column respectively, and a total of 9 rebars were embedded.

The construction process of the specimens is shown in Fig. 3a. When this method is used to strengthen the damaged columns for structural retrofitting, as the column top and column bottom are connected to other parts of the structure, the steel tube cannot be installed vertically. To solve this problem, two formed steel plates with the grouting hole are welded to a complete whole around the damaged column. In order to ensure the grouting quality, the SCC is carried out section by section. The SCC is first

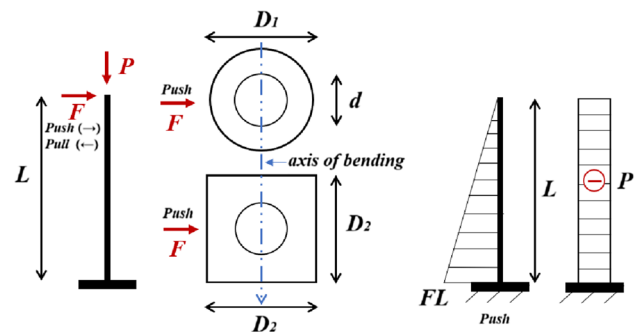


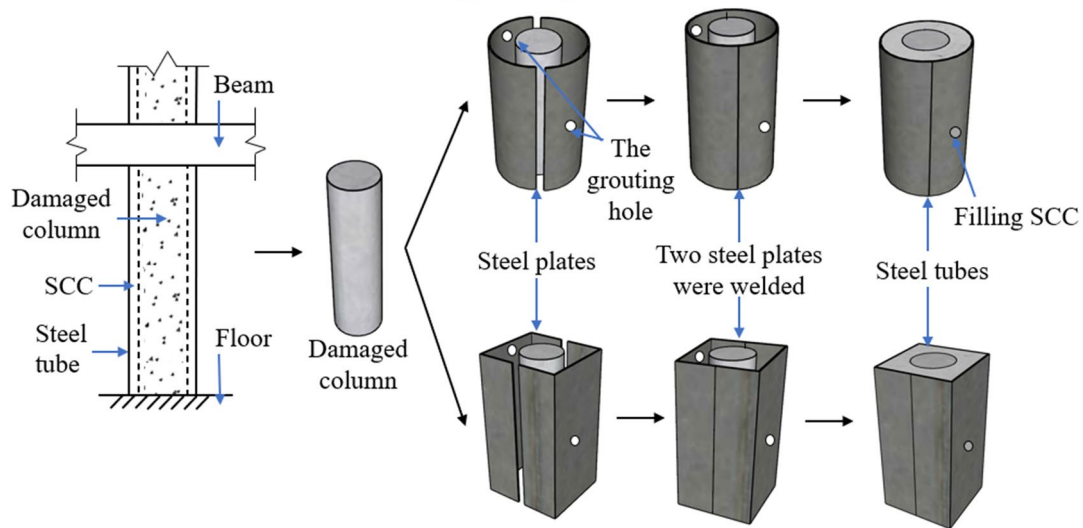
Fig. 2 Diagram of the reference structure

Table 1 Basic parameters of specimens

Specimens	D (mm)	L (mm)	T (mm)	Section shape	n (%)	N (%)
RC-1	110	1200	–	–	0.12	–
SC-1	200	1200	3.5	Square	0.12	–
SC-2	200	1200	3.5	Square	0.12	0.10
SC-3	200	1200	3.5	Square	0.12	0.06
SC-4	200	1200	3.5	Square	0.18	–
SC-5	200	1200	3.5	Square	0.06	–
CC-1	218	1200	3.5	Circular	0.12	–
CC-2	218	1200	3.5	Circular	0.24	–
CC-3	218	1200	3.5	Circular	0.18	–



(a) Test specimens



(b) Actual engineering

Fig. 3 Construction process

injected from the grouting hole in the middle, and then injected from the upper grouting hole after the previous hole is sealed. The construction process of the actual engineering is given in Fig. 3b.

2.2 Material Properties

The original RC column and RC footing were constructed with commercial concrete with a grade of 25 MPa, and the

SCC with a grade of 20 MPa was poured between the original RC column and the steel tube. Based on the Chinese standard GBT 50081-2010 (2010), the compressive tests were performed on ten standard cubes in two groups. The strength of commercial concrete and SCC were determined as 17.4 and 23.4 MPa, respectively. The elasticity modulus of commercial concrete and SCC were determined as 23,855 and 27,119 GPa, respectively. 3.5 mm thick steel tubes, 8 and 12 mm longitudinal rebars with grade HPB300, and 6 mm hoop rebars with grade HRB335 were adopted in the fabrication of specimens. According to the Chinese standard GBT 228.1-2010 (2010), the tensile tests were performed with 2 mm/min loading rate on each reserved standard sample. The properties of steel is listed in Table 2.

2.3 Test Setup and Loading System

As depicted in Fig. 4a, the lateral force was applied to the top of specimens via a maximum range of 1000 kN hydraulic servo actuator, and the same hydraulic servo actuator was adopted to apply axial loads at the top of specimens. The RC footing was connected to the ground with four bolts to ensure the stability of specimens. Three linear voltage differential transducers (LVDT) with a maximum range of 100 mm were arranged at the top height, middle height, and 1/4 height of

the column to monitor displacement. Besides, three LVDTs were placed at the RC footing to measure the lateral slippage of specimens. The strain gauges of the longitudinal rebars of the RC columns were pasted within 60 mm from the column bottom, and the strain gauges of the longitudinal rebars and steel tubes of the SCFST strengthened column were pasted within 100 mm from the column bottom.

The displacement-control system was adopted to apply lateral force. The displacement-control loading protocol was conducted according to the Chinese standard JGJ T101-2015 (2015). The lateral displacement was applied one cycle in 2 mm, 4 mm and 6 mm stage. Then, it was loaded with an increase of 2 mm step by step, and each cycle was repeated three times. The test was terminated when the load dropped to less than 85% of the peak load. Figure 4b depicts the loading procedure of the test. Herein, Δ_y is 2 mm.

3 Failure Modes

3.1 The Original RC Column

The failure of specimen RC-1 was bending shear failure. It was in an elastic stage and no obvious cracks were found at the early stage. When the displacement attained 10 mm, transverse cracks were generated at 60 mm from the column bottom. With the lateral displacement increasing, transverse cracks exhibited a tendency of extension and the concrete surface emerged some new cracks. As shown in Fig. 5a, approaching the loading displacement of 20 mm, the initial cracks at column bottom tended to be visible and formed a circumferential crack, more transverse and vertical cracks were generated at the column bottom, and concrete spalling was observed. Meanwhile, strain gauges of the longitudinal bars at column bottom exceeded $2000 \mu\epsilon$. Along with the loading level increasing, both the number and width of cracks increased, the positions of cracks developed along

Table 2 Steel material properties

Specimen	Yield strength (f_y /Mpa)	Tensile strength (f_t /Mpa)	Elasticity modulus (E_s /Gpa)
6 mm rebar	416	515	195
8 mm rebar	421	566	199
12 mm rebar	415	590	206
Square steel tube	485	585	188
Circular steel tube	365	490	171

Fig. 4 Test arrangement

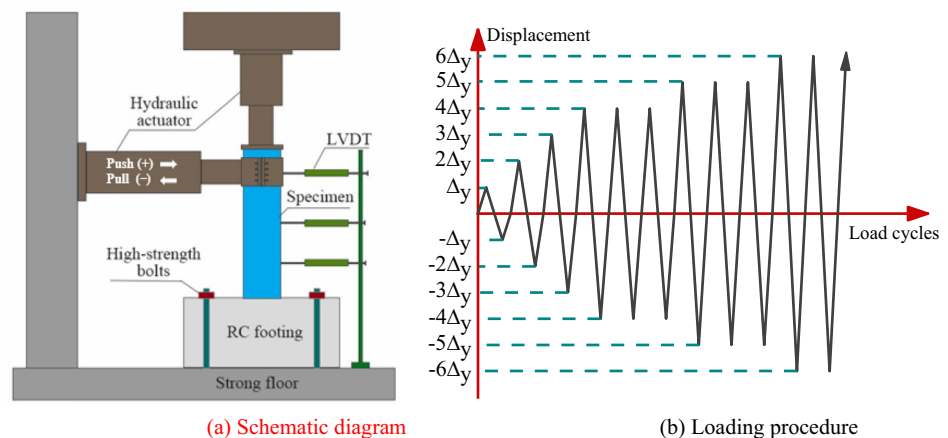




Fig. 5 Failure modes of the specimens

the column height gradually, and concrete peeled off significantly. When the lateral displacement reached 30 mm, the bearing capacity of specimen RC-1 was completely lost owing to the severe damage of column bottom.

3.2 SCFST Strengthened Columns

The failure modes of strengthened columns is shown in Fig. 5b, c. Brittle failure of core concrete at base and separation of column bottom and RC footing are the main failure modes of SCFST strengthened columns. During the process of all test, no visible buckling on the steel tube was observed. The specific description as follow is based on specimen CC-1. When the specimen was applied to the designed axial force, the compressive strains at the longitudinal bars bottom

ranged from 100 to 200 $\mu\epsilon$, and the maximum compressive strain at the steel tubes bottom was only 12 $\mu\epsilon$. With the loading level increasing, the strains of steel tube and rebar increased continuously. At the initial stage, the column was in an elastic stage and no obvious cracks were observed. The microcracks were generated between the column bottom and RC footing within the lateral displacement of 6–8 mm. When the displacement reached to 16 mm, strain gauges of the longitudinal bars at column bottom exceeded 2000 $\mu\epsilon$. As the lateral displacement increased, the cracks exhibited a tendency to extend and even fracture accompanied with intermittent noise from steel tube. In the maximum displacement of 24 mm loading, the column bottom and RC footing were further separated, and it was measured that the width of separation distance reached 10 mm, as illustrated in Fig. 5c. Especially, when the displacement attained 14 mm, the test was terminated because of the serious inclination of specimen CC-2.

To investigate the damage to SCC, the outer steel tube was removed. As depicted in Fig. 5d, the slight damage to SCC occurred at column bottom, and SCC in other regions was smooth and flat without visible cracks. After knocking off the SCC, an intimate bond between SCC and original concrete was observed. It indicated that the steel tube can restrain the core concrete and the ability of cracks generated on core SCC along the column height was prevented.

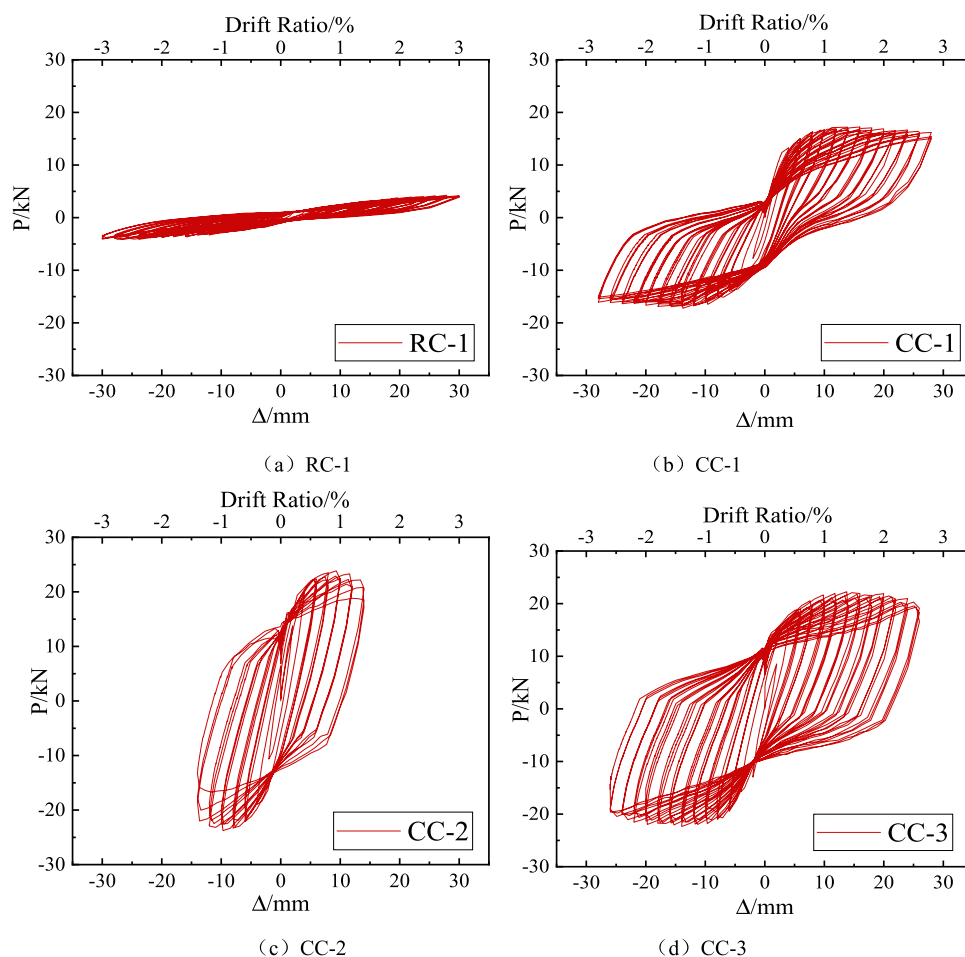
4 Results and Discussion

4.1 Hysteresis Behaviour

The hysteresis curves of all specimens were depicted in Fig. 6, respectively. Detailed analyses are as follows:

1. The strengthened columns showed better hysteresis behaviour and energy dissipation capacity. The hysteresis curve of specimen RC-1 exhibited inverse S-shape and a visible pinching phenomenon, which could be mainly attributed to the bond slippage occurred between rebars and concrete. The hysteresis loop of strengthened columns was plumper than that of specimen RC-1, and its slippage section was less than that of specimen RC-1. This was mainly because with the lateral displacement increasing, the tensile side of steel tube was separated from the basement, the lateral load was borne by the rebars and concrete, resulting the slippage of the bars connecting the column and the basement. As shown in Fig. 6a, e, the peak load of specimen SC-1 was 5.4 times that of specimen RC-1, implying that the bearing capacity of strengthened columns showed an excellent enhancement compared with the unstrengthened column. The reasons were chiefly as follows. The old

Fig. 6 Hysteresis curves of specimens



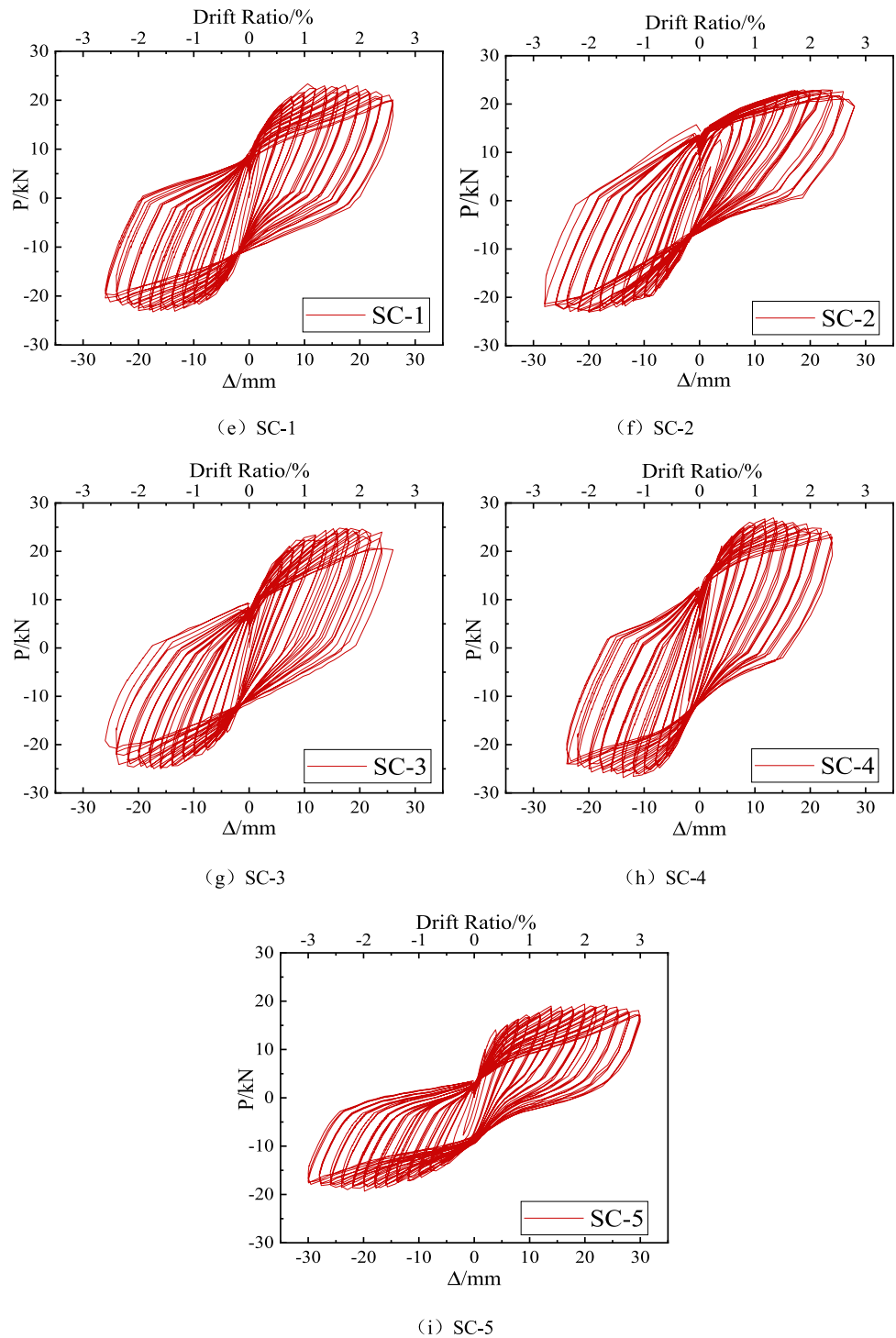
concrete was wrapped by the new concrete, and the surface of new concrete and steel tube formed the interface bond. With the displacement increasing, the restraint provided by steel tubes made the concrete in a state of triaxial compressive stress. The slippage between rebar and old concrete was inhibited by strengthening under same loading level. Thus, the bearing capacity and deformability were improved.

- As depicted in Fig. 6b–e, h, i, the peak load of specimen SC-4 was 17% and 39% higher than that of specimens SC-1 and SC-5, respectively. Compared with specimens CC-3 and CC-1, the peak load of specimen CC-2 increased by 6% and 38%, respectively. It can be concluded that with the increase of designed axial compression ratio, the bearing capacity was enhanced accordingly. The cause might be that the separation between the strengthened column bottom and RC footing was observed, and the longitudinal rebars of the original RC column were tensioned. A moderate increase in axial compression ratio could inhibit the yield of longitudinal rebars and thus enhance the bearing capacity. Besides, with the designed axial compression ratio increasing, the constraint effect of steel tube on the core concrete

was more obvious, resulting in greater bearing capacity. However, the existing studies (Foraboschi, 2020) showed that the interaction between flexure and axial force had to account for the effects of loads acting on the deformed structure. when the axial compression ratio was large, the steel tube did not have enough ability to restrain the core concrete, and compression failures of core concrete and the effects of loads were aggravated. It indicated the bearing capacity could be improved only when the axial compression ratio was increased within a certain range.

- As illustrated in Fig. 6b, d, e, h, the bearing capacity of SCFSST strengthened columns were higher than that of SCFCST strengthened columns. The peak load of specimen SC-1 increased by 34% compared with specimen CC-1, the peak loads of specimen SC-4 increased by 21% compared with specimen CC-3. This can be explained as follows. The hoop coefficient ξ of the SCFSST strengthened column was approximately 1.3 times that of the SCFCST strengthened column, which improved the restraint effect of steel tube on core concrete. Further, the section strength contributed by the square steel tube was higher than that contributed by the

Fig. 6 (continued)



circular steel tube, as shown in Sect. 4.5. Here, $\xi = A_s f_y / A_c f_{ck}$, $\xi_{SCFSST} = 2.27$, $\xi_{SCFCST} = 1.74$, A_s is section area of steel tube, A_c is section area of concrete, f_y is yield strength of steel, f_{ck} is standard value of compressive strength of concrete.

4. The embedding rebars ratios of specimens SC-2 and SC-3 were 0.10% and 0.06%, respectively. It can be seen from Fig. 6e–g that the peak load of specimen SC-3

was 7.5% higher than that of specimen SC-1, but the peak loads of specimens SC-2 and SC-1 were almost the same. It indicated that embedding an appropriate amount of rebars slightly could strengthen the connection between the old and new concrete, which can improve the strength of the bottom concrete and the shear capacity and bearing capacity of the specimen. When the embedding rebars ratio was overly high, seri-

ous damage to the original RC column surface was generated in the process of drilling holes, resulting in a decrease of reinforcement effect.

$$K_i = \frac{|+F_i| + |-F_i|}{|+X_i| + |-X_i|} \tag{1}$$

where $+F_i$ and $-F_i$ represent the positive and negative peak load corresponding to the peak point on the hysteretic loop of first cycle at i displacement, respectively. The $+X_i$ and $-X_i$ are the corresponding displacements.

4.2 Stiffness

The equivalent stiffness K_i is employed to compare the stiffness degradation under various levels of loading. The equivalent stiffness K_i could be expressed as:

It could be found from Fig. 7a that the equivalent stiffness of specimen SC-1 was significantly greater than that of the unstrengthened column in each stage, and the initial

Fig. 7 Stiffness degradation curves of specimens. **a** Strengthening effect, **b** Axial compression ratio of SCFSST columns, **c** Axial compression ratio of SCFCST columns, **d** Cross-section shape, **e** Rebars implantation ratio

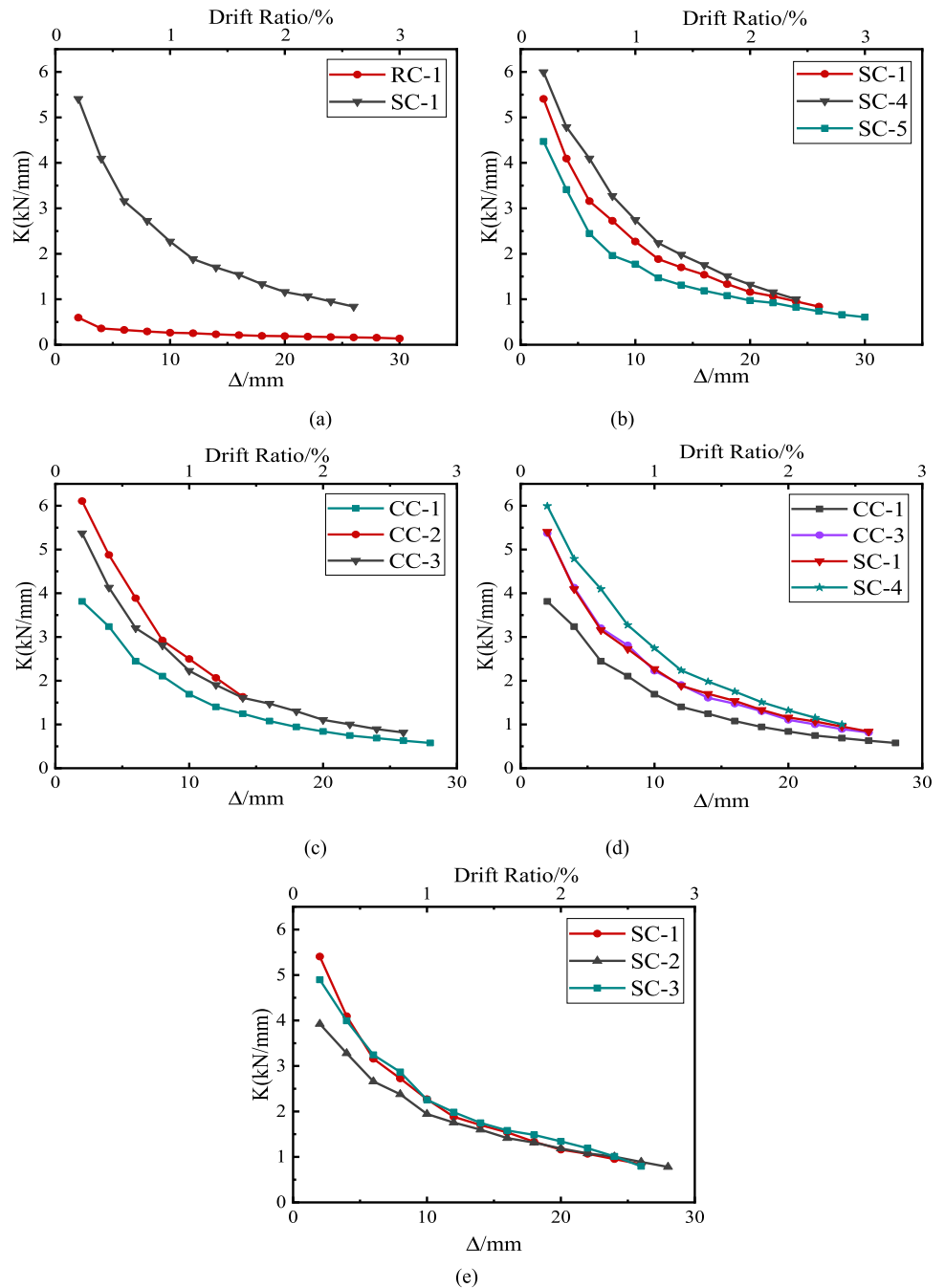


Table 3 Feature points of specimens and displacement ductility coefficients

Specimen	Δ_y/mm		P_y/kN		Δ_u/mm		μ		Averag value
	Forward	Reverse	Forward	Reverse	Forward	Reverse	Forward	Reverse	
RC-1	15.74	- 15.01	3.20	- 3.42	28.00	- 28.00	1.78	1.87	1.82
SC-1	6.94	- 5.95	19.92	- 18.91	26.00	- 26.00	3.75	4.37	4.06
SC-2	9.63	- 8.98	18.74	- 19.32	28.00	- 28.00	2.91	3.12	3.01
SC-3	7.50	- 7.19	21.17	- 20.81	26.00	- 26.00	3.46	3.61	3.54
SC-4	6.04	- 6.46	23.03	- 23.76	24.00	- 24.00	3.97	3.71	3.84
SC-5	6.46	- 7.10	15.36	- 14.64	30.00	- 30.00	4.64	4.23	4.44
CC-1	7.18	- 6.98	15.80	- 15.14	28.00	- 28.00	3.90	4.01	3.96
CC-2	4.42	- 4.97	20.71	- 20.48	14.00	- 14.00	3.17	2.82	2.99
CC-3	6.87	- 7.06	19.82	- 20.66	26.00	- 26.00	3.78	3.68	3.73

equivalent stiffness of specimen SC-1 was 9.08 times that of the unstrengthened column. The stiffness degradation curve of all strengthened columns showed an obvious downward trend, and the decrease of equivalent stiffness of the unstrengthened column can be neglected. The main reason for this phenomenon was as follows. During the loading progress, the unstrengthened column was subject to ductile failure. For the strengthened columns, the wrapping of steel tube made concrete cracks not occur along the column height, but only between the column bottom and RC footing, and slippage occurred between rebars connecting the column and the basement. With the increase of displacement, the slippage and crack expansion of strengthened columns were completed, and the degradation degree of stiffness slowed down.

As shown in Fig. 7b, c, with the axial compression ratio increasing, the equivalent stiffness of both SCFCST strengthened columns and SCFSST strengthened columns increased, and the initial K of strengthened columns increased by 21–60%. However, the K of specimen SC-1 increased by 42.11% compared with specimen CC-1, and the K of specimen SC-4 increased by 11.73% compared with specimen CC-3, as depicted in Fig. 7d. It can be concluded that the square steel tube with a higher hoop coefficient exhibited a better restrain effect. As shown in Fig. 7e, the smaller embedding rebars ratio had minor influence on the stiffness degradation of the specimen. Compared with SC-1 and SC-3, the K of the specimen SC-2 with the largest embedding rebars ratio was the smallest at each loading stage. It indicated large embedding rebars ratio could aggravate stiffness degradation.

4.3 Ductility

The displacement ductility μ is employed to further analyze, and the position of yield point and the corresponding load and displacement on the skeleton curve are determined by the R.

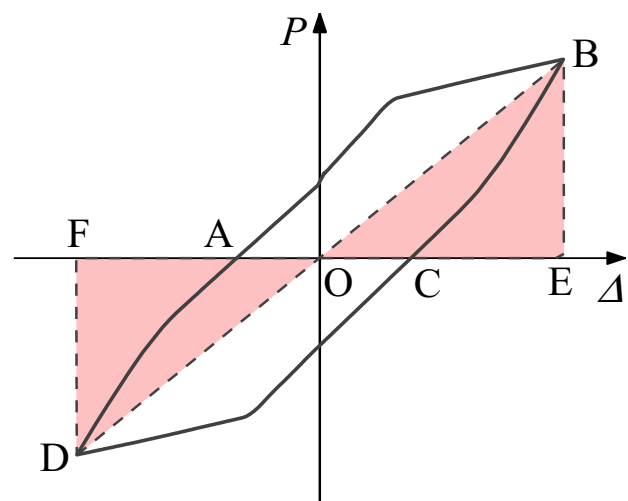


Fig. 8 Equivalent viscous damping coefficient calculation diagram

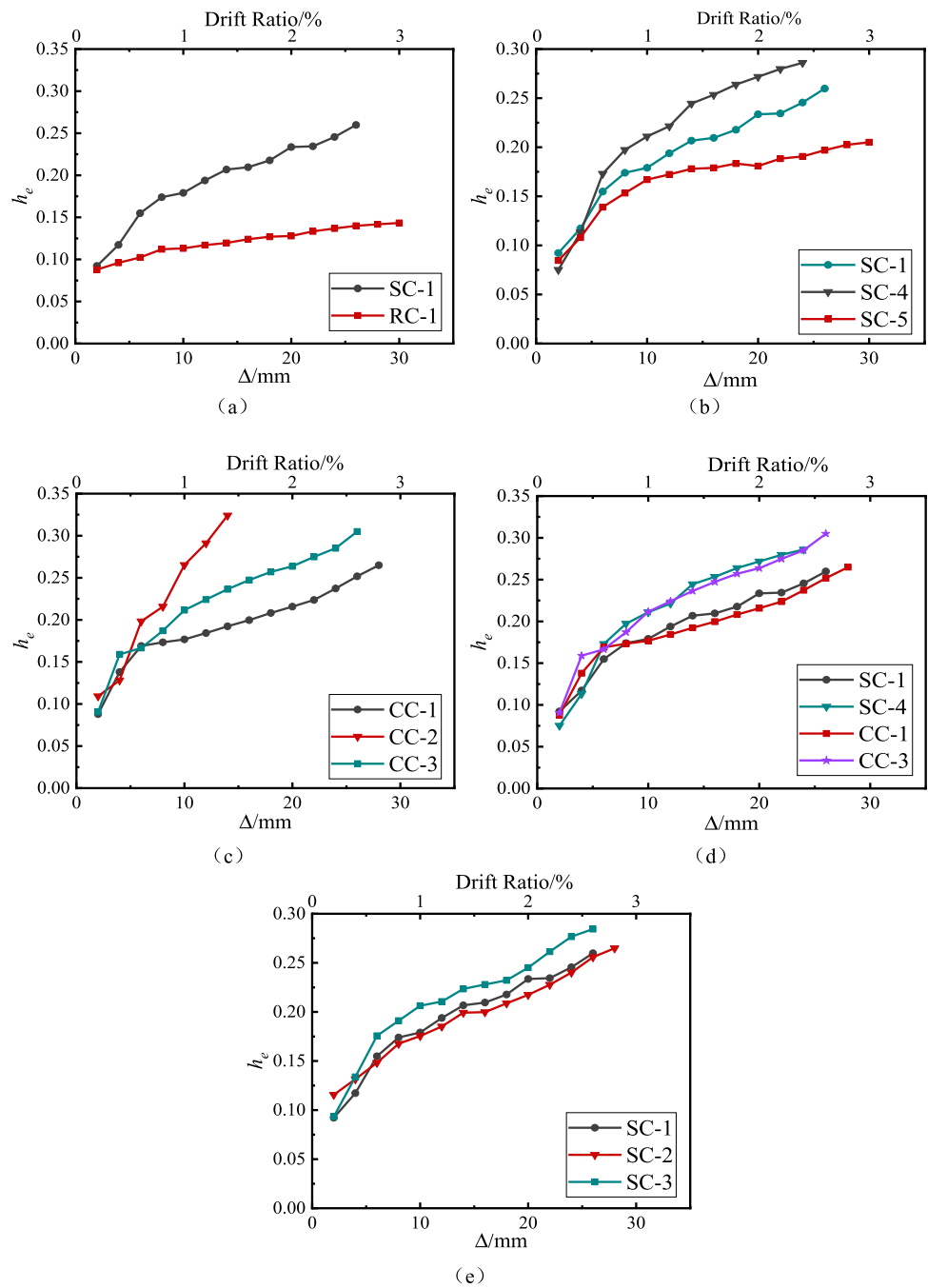
Park method (Wu et al., 2017). The μ could be calculated as follows:

$$\mu = \Delta_u / \Delta_y \tag{2}$$

where, Δ_u represents ultimate displacement, Δ_y represents yield displacement.

Table 3 summarizes the feature points of specimens and displacement ductility coefficient μ . The μ of specimen SC-1 was approximately enhanced by 123% in comparison to the unstrengthened column, indicating that the reinforcement method using in this paper could significantly improve the ductility. Furthermore, compared with specimen SC-5, the μ of specimens SC-1 and SC-4 decreased by 8.56% and 15.63% respectively, and the μ of specimens CC-1, CC-2 and CC-3 were 3.96, 2.99, 3.73 respectively. It can be concluded from those comparisons that the P-Δ effect was enhanced with the increase of axial force, which eventually led to the decrease of ductility. The μ of specimen SC-1 increased by

Fig. 9 Variation curves of equivalent viscous damping coefficients of specimens. **a** Strengthening effect, **b** Axial compression ratio of SCFSST columns, **c** Axial compression ratio of SCFCST columns, **d** Cross-section shape, **e** Rebars implantation ratio



2.53% compared with specimen CC-1, and the μ of specimen SC-4 increased by 2.95% compared with specimen CC-3. It indicated the cross-sectional shape had a slight effect on the improvement of ductility. Additionally, the μ of specimens SC-3 and SC-2 decreased by 12.81% and 25.86% compared with specimen SC-1, respectively. It indicated the μ was descended with the embedding rebars ratio increasing.

4.4 Energy Dissipation

The equivalent viscous damping coefficient h_e is adopted to describe the energy dissipation capacity (Guan et al., 2021; Mou et al., 2021). The calculation formula (JGJ/T. 101–2015, 2015) could be defined as follows:

$$h_e = \frac{1}{2\pi} \times \frac{S_{(ABC+CDA)}}{S_{(OBE+ODF)}} \tag{3}$$

where, as shown in Fig. 8, S_{ABC} and S_{CDA} are the areas of ABC and CDA of hysteresis curve, respectively; S_{OBE} and S_{ODF} are triangle areas of OBE and ODF , respectively.

As illustrated in Fig. 9a, the h_e of specimen SC-1 in the final stage increased by 85.7% compared with the unstrengthened column, it indicated that the strengthening method had a significant impact on the improvement of energy dissipation capacity. The SCFSST strengthened columns exhibited slightly outstanding reinforcement effect compared with the SCFCST strengthened columns, as shown in Fig. 8d. A significant improvement in equivalent viscous damping coefficient owing to the increase in axial compression ratio can be seen from Fig. 9b, c and the h_e in the final stage increased by 15–40% compared to the specimen with the smallest axial compression ratio. As shown in Fig. 9e, there was little difference between the h_e of specimen SC-1 and specimen SC-2 in each stage, and the h_e curve of specimen SC-3 was basically above that of specimens SC-1 and SC-2. Especially, the h_e of specimen SC-3 in the final stage increased by 9.31% compared with specimen SC-1. It indicated the energy dissipation capacity of strengthened columns was enhanced by embedding an appropriate amount of rebars. In conclusion, Fig. 9 had the same scale of the coordinate axis, it could be clearly seen that the axial compression ratio had the greatest influence on the energy dissipation capacity of the specimens among the three parameters.

4.5 Evaluation of Section Strength

To obtain the strength contribution of components, according to the Chinese standard JGJT 471–2019 (2019), the section strength was evaluated as the following formula.

$$N_{cc} = A_{cc}f_{cc} + A_b f_b f_{cc} = f_c + 5.1f_{el} \tag{4}$$

$$f_c = \frac{f_{c1}A_{c1} + f_{c2}A_{c2}}{A_{c1} + A_{c2}} \tag{5}$$

For SCFCST strengthened columns:

$$f_{elc} = \frac{2k_s k_h t f_t}{D} \tag{6}$$

For SCFSST strengthened columns:

$$f_{els} = \frac{2k_s k_h t f_t}{D} \tag{7}$$

$$k_h = -\frac{h_t}{D} + 1 \tag{8}$$

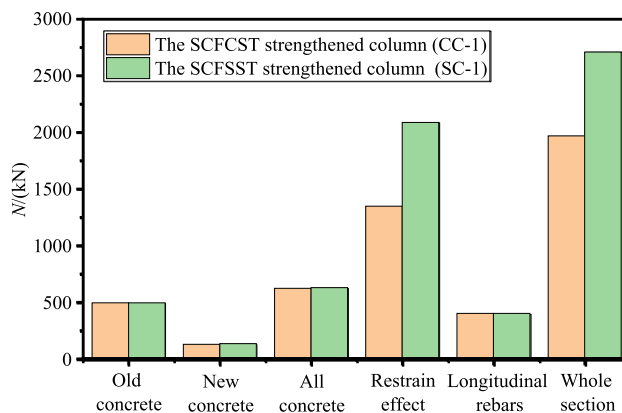


Fig. 10 The contribution of section strength

$$k_s = \frac{27t}{D} \sqrt{\frac{f_t}{235}} \left(\frac{30}{f_c} \right) \tag{9}$$

where, N_{cc} is the loads shared by the specimen; A_{cc} and A_b are the area of restrained concrete and longitudinal rebars, respectively; f_{cc} and f_b are the axial compressive strength of restrained concrete and longitudinal rebars; f_c is the converted axial compressive strength of new and old concrete; f_{c1} and f_{c2} indicate the axial compressive strength of new and old concrete; f_{elc} and f_{els} indicate the equivalent restraint stress of steel tubes; k_s and k_h are the restraint coefficient of section and height of steel tubes; f_t is the tensile strength of steel tubes; t is the thickness of steel tubes; D represents the diameter or side length of steel tubes.

The representative specimens SC-1 and CC-1 were selected for comparison. The contribution of section strength is depicted in Fig. 10. It indicated the section strength of the SCFSST strengthened column was obviously greater than that of the SCFCST strengthened column. In particular, the section strength contributed by the square steel tube increased by 54.94% compared to that contributed by the circular steel tube.

5 Conclusions

In this paper, the study on the seismic performance of RC circular columns strengthened with self-compacting concrete-filled steel tubes was presented. The primary conclusions are as follows:

1. The unstrengthened column suffered bending shear failure, and cracks were generated along the column height. Due to the restraint provided by steel tube prevented the occurrence of concrete cracks along column height,

the main failure mode of strengthened columns was the separation between column bottom and basement.

- The specimen exhibited better seismic behavior by strengthening with SCFST. The bearing capacity and stiffness of the strengthened column were 5.4 and 9.08 times than that of the unstrengthened column respectively, and the improvement ratio of ductility and energy dissipation reached 123 % and 85.7% respectively. The bearing capacity and stiffness of the SCFSST strengthened column were greater than that of the SCFCST strengthened column.
- With the designed axial compression ratio increasing, the bearing capacity, initial stiffness, and energy dissipation capacity of strengthened columns increased by 17–39%, 21–60%, and 15–40% respectively, but the ductility coefficient decreased by 8.56–32.4%. The bearing capacity, stiffness, and energy dissipation capacity of strengthened columns could be slightly enhanced by embedding an appropriate amount of rebars. When the embedding rebars ratio was large, the reinforcement effect can be basically negligible.
- The evaluation of section strength indicated that SCF-SST strengthened columns had greater section strength, and the section strength contributed by the square steel tube increased by 54.94% compared to that contributed by the circular steel tube, as the equivalent restraint stress of square steel tubes greater than that of circular steel tubes.

Acknowledgements This study was financially supported by the Natural Science Foundation of Sichuan Province (Grant no. 2022NSFSC0319 and 2022NSFSC0095), the Science and Technology Research Projects of Mianyang, China (Grant no. 15S-02-3).

Declaration

Conflict of interest We declare that we do not have any commercial or associative interest that represents a conflict of interest in connection with the work submitted.

References

- Abdalla, S., Abed, F., & AlHamaydeh, M. (2013). Behavior of CFSTs and CCFSTs under quasi-static axial compression. *Journal of Constructional Steel Research*, 90, 235–244. <https://doi.org/10.1016/j.jcsr.2013.08.007>
- Abed, F., AlHamaydeh, M., & Abdalla, S. (2013). Experimental and numerical investigations of the compressive behavior of concrete filled steel tubes (CFSTs). *Journal of Constructional Steel Research*, 80, 429–439. <https://doi.org/10.1016/j.jcsr.2012.10.005>
- Foraboschi, P. (2013). Layered plate with discontinuous connection: Exact mathematical model. *Composites Part B: Engineering*, 47, 365–378. <https://doi.org/10.1016/j.compositesb.2012.11.004>
- Foraboschi, P. (2020). Predictive formulation for the ultimate combinations of axial force and bending moment attainable by steel members. *International Journal of Steel Structures*, 20, 705–724. <https://doi.org/10.1007/s13296-020-00316-6>
- G.B. 50011-2010 (2010) Code for design of concrete structures. China Architecture Building Press, Beijing.
- G.B./T 50081 (2010). Standard for Test Methods of Physical and Mechanical Properties of Concrete. China Architecture Building Press, Beijing.
- Gan, D., Zhou, X., Liu, J., & Li, J. (2015). Composite response of circular tubed reinforced concrete short columns under cyclic lateral load. *Journal of Building Structures*, 36(S1), 222–229. <https://doi.org/10.14006/j.jzjgxb.2015.S1.034>. (in Chinese).
- Guan, D., Chen, Z., Liu, J., Lin, Z., & Guo, Z. (2021). Seismic performance of precast concrete columns with prefabricated UHPC jackets in plastic hinge zone. *Engineering Structures*, 245, 112776. <https://doi.org/10.1016/j.engstruct.2021.112776>
- Han, L., Lin, X., & Wang, Y. (2006). Cyclic performance of repaired concrete-filled steel tubular columns after exposure to fire. *Thin-Walled Structures*, 44, 1063–1076. <https://doi.org/10.1016/j.tws.2006.10.001>
- Han, L., Yao, G., & Zhao, X. (2005). Tests and calculations for hollow structural steel (HSS) stub columns filled with self-consolidating concrete (SCC). *Journal of Constructional Steel Research*, 61(9), 1241–1269. <https://doi.org/10.1016/j.jcsr.2005.01.004>
- He, A., Cai, J., Chen, Q. J., Liu, X. P., Huang, P. Z., & Tang, X. L. (2018). Seismic behavior of steel-jacket retrofitted reinforced concrete columns with recycled aggregate concrete. *Construction and Building Materials*, 158, 624–639. <https://doi.org/10.1016/j.conbuildmat.2017.10.053>
- He, A., Cai, J., Chen, Q. J., Liu, X. P., & Xu, J. (2017). Axial compressive behavior of steel-jacket retrofitted RC columns with recycled aggregate concrete. *Construction and Building Materials*, 141, 501–516. <https://doi.org/10.1016/j.conbuildmat.2017.03.013>
- JGJ/T. 101-2015 (2015) Specification for seismic test of buildings. China Architecture Building Press, Beijing.
- JGJT. 471-2019 (2019) Technical standard for steel tube confined concrete structures. China Architecture Building Press, Beijing.
- Jiang, C., Wu, Y. F., & Wu, G. (2014). Plastic hinge length of FRP-confined square RC columns. *Journal of Composites for Construction*, 18, 1–12. [https://doi.org/10.1061/\(ASCE\)CC.1943-5614.0000463](https://doi.org/10.1061/(ASCE)CC.1943-5614.0000463)
- Karimipour, A., Ghalehnovi, M., Brito, J., & Attari, M. (2020). The effect of polypropylene fibers on the compressive strength, impact and heat resistance of self-compacting concrete. *Structures*, 25, 72–87. <https://doi.org/10.1016/j.istruc.2020.02.022>
- Li, W., Liang, H., Lu, Y., Xue, J., & Liu, Z. (2019). Axial behavior of slender RC square columns strengthened with circular steel tube and sandwiched concrete jackets. *Engineering Structures*, 179, 423–437. <https://doi.org/10.1016/j.engstruct.2018.11.018>
- Liao, J., Li, Y., Yi, O., & Zeng, J. (2021). Axial compression tests on elliptical high strength steel tubes filled with self-compacting concrete of different mix proportions. *Journal of Building Engineering*, 40, 102678. <https://doi.org/10.1016/j.job.2021.102678>
- Lu, Y., Liang, H., Li, S., & Li, N. (2015a). Axial behavior of RC columns strengthened with SCC filled square steel tubes. *Steel & Composite Structures*, 18(3), 623–639. <https://doi.org/10.12989/scs.2015.18.3.623>
- Lu, Y., Liang, H., Li, S., & Li, N. (2015b). Eccentric strength and design of RC columns strengthened with SCC filled steel tubes. *Steel & Composite Structures*, 18(4), 833–852. <https://doi.org/10.12989/scs.2015.18.4.833>
- Lu, Y., Yi, S., Li, S., & Zhao, X. (2018). Effect of the outer diameter on the behavior of square RC columns strengthened with self-compacting concrete filled circular steel tube. *International*

- Journal of Steel Structures*, 39(10), 65–74. <https://doi.org/10.1007/s13296-018-0185-9>
- Lu, Y., Yi, S., Liang, H., Gong, T., & Li, N. (2018). Seismic behavior of RC square columns strengthened with self-compacting concrete-filled CFRP-steel tubes. *Journal of Bridge Engineering*, 24(2), 04018119. [https://doi.org/10.1061/\(ASCE\)BE.1943-5592.0001345](https://doi.org/10.1061/(ASCE)BE.1943-5592.0001345)
- Mou, B., Liu, X., & Sun, Z. (2021). Seismic behavior of a novel beam to reinforced concrete-filled steel tube column joint. *Journal of Constructional Steel Research*, 187, 106931. <https://doi.org/10.1016/j.jcsr.2021.106931>
- Murugan, K., & Sengupta, A. K. (2020). Seismic performance of strengthened reinforced concrete columns. *Structures*, 27, 487–505. <https://doi.org/10.1016/j.istruc.2020.05.059>
- Priestley, M., Seible, F., Yan, X., & Verma, R. (1994a). Steel jacket retrofitting of reinforced concrete bridge columns for enhanced shear strength-part 1: Theoretical considerations and test design. *ACI Structural Journal*. <https://doi.org/10.14359/9885>
- Priestley, M., Seible, F., & Yan, X. (1994b). Steel jacket retrofitting of reinforced concrete bridge columns for enhanced shear strength-Part 2: Test results and comparison with theory. *Structural Journal*, 91(5), 537–551. <https://doi.org/10.14359/4168>
- Sezen, H., & Miller, E. A. (2011). Experimental evaluation of axial behavior of strengthened circular reinforced-concrete columns. *Journal of Bridge Engineering*, 16(2), 238–247. [https://doi.org/10.1061/\(asce\)be.1943-5592.0000143](https://doi.org/10.1061/(asce)be.1943-5592.0000143)
- Shannag, M. J., Barakat, S., & Abdul-Kareem, M. (2002). Cyclic behavior of HPRC-repaired reinforced concrete interior beam-column joints. *Materials and Structures*, 35, 348–356. <https://doi.org/10.1007/BF02483154>
- Tam, V. W. Y., Wang, Z. B., & Tao, Z. (2014). Behaviour of recycled aggregate concrete filled stainless steel stub columns. *Materials and Structures*, 47, 293–310. <https://doi.org/10.1617/s11527-013-0061-1>
- Valipour, H. R., & Foster, S. J. (2010). Nonlinear static and cyclic analysis of concrete-filled steel columns. *Journal of Constructional Steel Research*, 66(6), 793–802. <https://doi.org/10.1016/j.jcsr.2009.12.011>
- Wang, F., Wang, J., Yang, H., & Shen, Q. (2021). Axial compressive behavior of RC columns strengthened with rectangular steel tube and cementitious grout jackets. *Structures*, 31, 484–499. <https://doi.org/10.1016/j.istruc.2020.10.063>
- Wang, J., Sun, Q., & Li, J. (2019). Experimental study on seismic behavior of high-strength circular concrete-filled thin-walled steel tubular columns. *Engineering Structures*, 182, 403–415. <https://doi.org/10.1016/j.engstruct.2018.12.098>
- Wu, C., Pan, Z., Su, R. K. L., Leung, C. K. Y., & Meng, S. (2017). Seismic behavior of steel reinforced ECC columns under constant axial loading and reversed cyclic lateral loading. *Materials and Structures*, 50, 78. <https://doi.org/10.1617/s11527-016-0947-9>
- Xue, J., Lu, Y., Liang, H., & Gong, T. (2014). Research on bearing capacity of RC circular stub column strengthened with self-compacting concrete-filled circular steel tube under axial loading. *Engineering Journal of Wuhan University*, 47(06), 769–773. (in Chinese).
- Yan, Y., Liang, H., Lu, Y., Liu, Z., & Gong, T. (2019). Behavior of RC columns strengthened with SCC-filled steel tubes under cyclic loading. *Engineering Structures*, 199, 109603. <https://doi.org/10.1016/j.engstruct.2019.109603>
- Yu, X., Tao, Z., & Song, T. Y. (2016). Effect of different types of aggregates on the performance of concrete-filled steel tubular stub columns. *Materials and Structures*, 49, 3591–3605. <https://doi.org/10.1617/s11527-015-0742-z>
- Zhou, X., Zhang, S., & Liu, J. (2008). Seismic behavior of steel tube confined reinforced concrete (RC) beam-columns. *Journal of Building Structures*, 5, 75–84. <https://doi.org/10.14006/j.jzjgxb.2008.05.010>. (in Chinese).

Publisher's Note Springer Nature remains neutral with regard to jurisdictional claims in published maps and institutional affiliations.

Springer Nature or its licensor (e.g. a society or other partner) holds exclusive rights to this article under a publishing agreement with the author(s) or other rightsholder(s); author self-archiving of the accepted manuscript version of this article is solely governed by the terms of such publishing agreement and applicable law.